Chapter 1

Lipatov's Legacy and the Future of Deep Inelastic Scattering

1.1 Introduction

Around 1993-4, as a PhD student looking for an analysis topic using the first data from the world's only ever lepton-hadron collider facility, HERA, I became intrigued by the first observations [Derrick *et al.* (1993b); Ahmed *et al.* (1994)] of 'diffractive' deep inelastic scattering (DDIS, $ep \to eXp$) events in which the proton appeared to stay intact, despite the very large momentum transfer from the electron. Hearing about the mysterious 'pomeron' that was believed to mediate the process, I was completely hooked! In those early days, the questions we asked were relatively simple. Was this the 'soft' pomeron [Feinberg and Pomerančuk (1956)] that historically described elastic, total and soft diffractive cross sections, with some degree of universality [Kaidalov (1979); Goulianos (1983)], or was it a first sighting of a 'hard' pomeron, emerging as a high energy 'Regge' limit of QCD according to the work of Lev Nikolaevich Lipatov and others [Lipatov (1986, 1997)]. Searching for evidence for this QCD BFKL pomeron was a major theme throughout the lifetime of HERA and in some sense I am still working on it.

Applying the QCD pomeron to DDIS is only a small part of a much richer phenomenology that arises as a consequence of the BFKL equation [Kuraev *et al.* (1976, 1977); Balitsky and Lipatov (1978)], a differential equation in $\ln 1/x$ for an 'unintegrated' gluon density at asymptotically large energies. The unintegrated gluon density can be convoluted with off-mass-shell parton-level cross sections to make predictions for observables in the k_T factorisation scheme [Gribov *et al.* (1983); Levin *et al.* (1991); Catani *et al.* (1991); Collins and Ellis (1991)]. The corresponding pomeron emerges starting from a basic two-gluon exchange [Low (1975); Nussinov (1975)], developing into a 'ladder' with rungs corresponding via the optical theorem to x-ordered successive emissions of partons. As well as DDIS, the BFKL pomeron can be applied to predict energy dependences of inclusive deep inelastic scattering (DIS) $ep \to eX$ and quasi-elastic vector meson production $ep \to eVp$. Meanwhile, the properties of the hadronic final state of the inclusive DIS process are driven by the details of the parton cascade between the proton and the virtual exchange photon. Often at HERA, we (almost certainly naiively) framed physics

questions in terms of which of the two major evolution schemes was the dominant feature of the data; BFKL with its $\ln 1/x$ resummation and x ordering of partons, or DGLAP [Gribov and Lipatov (1972a,b); Lipatov (1975); Altarelli and Parisi (1977); Dokshitzer (1977)] with $\ln Q^2$ resummations and transverse momentum ordering. Whilst it is undoubtedly BFKL for which Lipatov is best known and most closely associated, it is a measure of his stature and contribution that he is the 'L' in both evolution schemes; the common link that joins the field together.

Whilst DGLAP evolution is fully accepted and widely used, BFKL is not yet well established in existing data, neither from HERA nor at the proton-proton energy frontier at the LHC. As a basic prediciton of QCD, it must ultimately exist; the question is where one needs to look. Large logarithms of $1/x$ play the central role and, through the kinematic correlation in electron-proton scattering $x = Q^2/sy$ where the kinematic variables have their usual meanings, large $1/x$ implies large centre of mass energy s. Given the dominance of the gluon density in low x proton structure, it seems apparent that low x DIS and BFKL physics are intimately linked. Searching for BFKL physics therefore sits, and will continue to sit, as a basic experimental question at the energy frontier of QCD.

This article describes low x physics aspects of future proposed DIS facilities. After a brief introduction to the currently proposed future faciltities, inclusive DIS, exclusive vector meson production, DDIS and final state studies are all reviewed, emphasising the role that might be played by Lipatov's work.

1.2 Possible Futures for Deep Inelastic Scattering

An overview of past, present and future electron-proton scattering facilties is shown in the plane of energy versus luminosity in figure 1.1. The only collider facility realised to date is HERA. It's large cente of mass energy opened up the field of low x physics. There are at present three proposals under discussion for future DIS collider facilities. The EIC and LHeC / FCC-eh both offer three orders of magnitude increases in luminosity over HERA, but have rather different physics focuses, commensuarate with their centre of mass energies. Whilst the EIC will operate with polarised protons and heavy ions to investigate 3 dimensional proton structure and nuclear effects, the LHeC and FCC-eh offer new phase space in ep physics towards higher $\sqrt{s}$ or equivalently low x. A third potential future facility, VHEeP is not shown in figure 1.1, but would extend the $\sqrt{s}$ or $1/x$ reach still further, albeit at low luminosities. These three proposed facilities are briefly described in the following. Their comparisons and complementarity are expanded in more detail in [Caldwell *et al.* (2018)].

1.2.0.1 *Electron-Ion Collider (EIC)*

Designs for a future high-luminosity polarised electron ion collider (EIC) have evolved in the past few years at Jefferson Laboratory and Brookhaven National

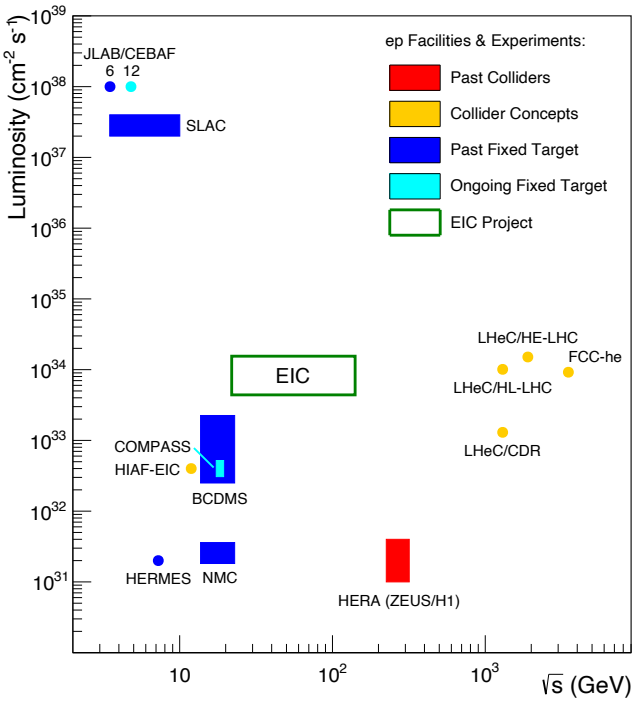

Fig. 1.1 Illustration [Ullrich (2019)] of the past, present and possible future landscape of DIS experiments in terms of *ep* centre of mass energy $\sqrt{s}$ versus instantaneous luminosity. VHEeP is not shown, but would sit in an energy range $1 < \sqrt{s} < 9$ TeV at luminosities up to the order of 10^{28} cm^{-2}s^{-1}.

Laboratory (BNL) in the United States [Accardi *et al.* (2016)]. The EIC project has recently received a major boost by attracting Department of Energy CD0 'mission need' approval, together with a site selection at BNL. It is therefore the most advanced of the future faciltities in terms of approval status and might be ready for data taking on a timescale of around 2030 at a cost of $\$1.6 - 2.6$ billion. The EIC will be realised by adding an electron storage ring to the existing RHIC heavy ion collider complex at BNL to enable electron-ion collisions. The forseen energy range is $20 < \sqrt{s} < 140$ GeV at luminosities of order 10^{34} cm^{-2}s^{-1}. The EIC design incorporates a wide range of beam energies and polarisations for protons, deuterons and ions, enabling an unprecedented nucleon and nuclear femtography program.

Since the EIC centre of mass energy is smaller than that of HERA, it is unlikely that its inclusive data will shed fresh light on low x energy-driven effects such as BFKL dynamics. However, it remains plausible that its much higher luminosity than that of HERA and extensive programme of investigating exclusive processes may reveal something that has previously been missed. The facility may also be sen-

sitive to density-driven (as distinct from energy-driven) low x effects such as parton saturation [Mueller (1990)], due to its extensive plans for electron-ion scattering, the density of partons being enhanced over the case for electron-proton scattering by a factor $A^{1/3}$.

1.2.0.2 *Large Hadron-electron Collider (LHeC) and Future Circular electron-hadron Collider (FCC-eh)*

The LHeC [Abelleira Fernandez *et al.* (2012); LHeC Study Group (2020)] is a proposal to add an intense 60 GeV electron beam to the LHC proton (and heavy ion) accelerator complex, enabling ep or eA collisions to take place at the same time as the ongoing pp, pA and AA programme. The electron beam is based on a racetrack energy-recovery linear accelerator (ERL) configuration, in which beams circulate three times through two 10 GeV linear accelerator structures before being brought into collision with one of the LHC proton beams and subsequently winding back down through the same structures, enabling energy recovery. The first step towards the LHeC is to build a lower energy prototype ('PERLE'), which is currently planned for Orsay [Angal-Kalinin *et al.* (2018)]. The LHeC reaches previously unexplored energies, (nominally $\sqrt{s} = 1300$ GeV) at high luminosity, 10^{34} cm^{-2}s^{-1}. Its future prospects depend on the overall strategy for paricle physics in Europe and worldwide. With a price tag of the order of CHF 1 Billion, its cost is an order of magnitude lower than currently discussed future energy frontier e^+e^- and pp collider projects. The LHeC physics programme is very broad; highlights include complementary characterisation of the Higgs boson to that at the LHC, reaching a new level of precision in proton PDF deteminations which, particularly at high x, will empower the LHC to extend its search programme to new particles with larger masses, as well as a major extension in kinematic range for the exploration of low x effects, as discussed here.

The FCC project [Abada *et al.* (2019)] is investigating the possibility and physics capabilities of adding a new 100 km circumference tunnel to the CERN infrastructure, housing electron or hadron beams. The hadron-hadron collider design (FCC-hh) could be complemented by an electron accelerator of similar design to that of the LHeC, enabling very high energy ep and eA collisions. The FCC-eh would increase the energy reach for electron-proton collisions to $\sqrt{s} = 3500$ GeV, again with luminosity of order 1.5×10^{34} cm^{-2}s^{-1}. Timescales for realisation are long and depend critically on the future direction of CERN's programme.

Integrated luminosities of order 1 ab^{-1} and 3 ab^{-1} are envisioned for the LHeC and FCC-eh, respectively. However, a low x programme can be realised with much smaller amounts of data. As described in [LHeC Study Group (2020)], the LHeC programme might be staged, with a first component overlapping with LHC operation and an extended programme taking place in standalone mode. An initial luminosity of 50 fb^{-1}, as envisioned for a three year 'LHeC First Run' programme during LHC run 5, would already be more than sufficient for the investigation of

the observables discussed in this document.

1.2.0.3 *Very-High Energy electron-proton collider (VHEeP)*

The VHEeP design [Caldwell and Wing (2016)] aims to exploit the highly encouraging progress made by the CERN AWAKE project [Edli *et al.* (2018)], in plasma wakefield acceleration. The existing 7 TeV per proton LHC bunches[1] are used as the driver for the protons to create a wakefield which then accelerates electrons to 3 TeV. The electrons then collide with the other LHC proton beam. The potential energy reach of the VHEeP design thus extends to $\sqrt{s} = 9000$ GeV, the highest values among current proposals. If sufficient beam stability can be achieved, luminosities of up to 10^{29} cm^{-2}s^{-1} have been predicted. Although this is only 1% of the maximum achieved by HERA, VHEeP would still be able to measure the ultra-high-energy behavior of hadronic cross sections in regions where new QCD dynamics must exist.

1.3 Phenomenology and Background from HERA

Much of low x physics, including the phenomenological implications of the BFKL pomeron, is concerned with energy dependences. These are conveniently expressed in terms of Regge phenomenology, which predates QCD and applies at asymptotically large $\sqrt{s}$. In terms of a 'pomeron' trajectory $\alpha(t) = \alpha(0) + \alpha' t$ with intercept $\alpha(0)$, elastic cross sections behave as $\mathrm{d}\sigma_{\mathrm{el}}/\mathrm{d}t \propto s^{2\alpha(t)-2}$ at fixed t and, via the optical theorem, total cross sections follow $\sigma_{\mathrm{tot}} \propto s^{\alpha(0)-1}$. In the context of DIS at modest Q^2, it is natural to think of the cross section for the inclusive neutral current DIS process $ep \to eX$ as factorising into a flux of virtual photons from the electron and a total $\gamma^* p$ cross section. The $\gamma^* p$ centre of mass energy W is related to the familiar kinematic variables of DIS via $W^2 = Q^2/x$. In Regge language, the total cross section at fixed Q^2 is thus expected to follow a power-law behaviour $\sigma_{\mathrm{tot}}^{\gamma^* p} \propto x^{-(\alpha(0)-1)}$ and may be discussed in terms of an effective pomeron intercept. Similarly, the forward (i.e. $t \to 0$) quasi-elastic cross section for exclusive vector meson production follows $\mathrm{d}\sigma_{\mathrm{EL}}^{\gamma^* p}/\mathrm{d}t \propto x^{-2(\alpha(0)-1)}$.

The 'soft' pomeron intercept, governing for example the slowly rising total pp and $\bar{p}p$ high energy cross sections, has been found to be a little larger than unity; for example the famous Dannachie and Landshoff simple pole analysis finds $\alpha(0) = 1.08 - 1.10$ [Donnachie and Landshoff (1992); Cudell *et al.* (1997)].[2] The solution to the BFKL evolution equation is a gluon density that grows with $1/x$ as a power, $x^{-\omega_{I\!P}}$, such that $1 + \omega_{I\!P}$ is the hard pomeron intercept. In the leading logarithmic approximation, $\omega_{I\!P} = 4\bar{\alpha}_s \ln 2$ and $\bar{\alpha}_s = 3\alpha_s/\pi$ for the three colours of QCD, such

[1] A similar scheme, using the CERN SPS accelerator as the proton driver, known as PEPIC, has also been suggested.

[2] Results from elastic and total cross sections at the LHC suggest a breakdown of this behaviour, possibly due to multi-Regge exchanges as discussed for example in [Khoze, D. and Ryskin, M and Tasevsky, M. (2020)].

that $\alpha(0) \simeq 1.5$, a much larger value than that for the soft pomeron. By analogy with the soft pomeron, the BFKL pomeron then provides a contribution to elastic, total and diffractive dissociation cross sections which can be characterised in the language of Regge phenomenology in terms of steeply rising cross sections with increasing energy. In particular, elastic cross sections at vanishing t are predicted to follow $\mathrm{d}\sigma_{\mathrm{EL}}^{\gamma^* p}/\mathrm{d}t \propto \left(W^2\right)^{2\omega_{I\!P}}$. For a detailed discussion, see e.g. [Forshaw and Ross (1997)].

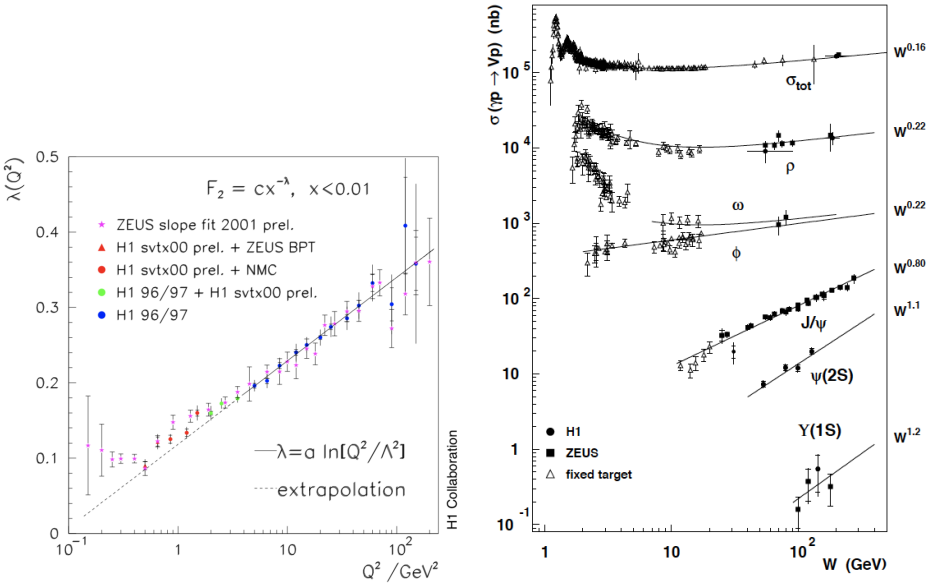

Fig. 1.2 Energy dependences for a subset of HERA data. (left) The Q^2 dependence of λ when inclusive DIS data are fitted to the form $F_2 \propto \sigma_{\mathrm{tot}}(\gamma^* p \to X) \propto x^{-\lambda}$ at each fixed Q^2 [Newman (2004)]. (right) W dependences for quasi-elastic vector meson photoproduction $\gamma p \to V p$ for different vector meson species, V. The results of power law fits of the form $\sigma \propto W^{\delta}$ are indicateed in each case [Levy (2009)].

When the first results on inclusive DIS emerged from HERA [Abt *et al.* (1993); Derrick *et al.* (1993a)] at intermediate $Q^2 \sim 10 - 100$ GeV^2, steep rises with decreasing x were observed for the first time, not explainable by the soft pomeron. Whilst not entirely unexpected from more traditional approaches [De Rujula *et al.* (1974)], this led to speculation that the hard pomeron was at work. However, matters became still more ingtriguing when Lipatov and co-authors published the masterful next-to-leading-logarithm (NLL) corrections to the BFKL equation, indicating strongly downward changes in $\omega_{I\!P}$ [Fadin and Lipatov (1998); Ciafaloni and Camici (1998)]. As discussed elsewhere in this book [Stasto, A. M. (2020)], there has since been a long process of understanding and ultimately resumming these corrections, leading to a picture where $\omega_{I\!P}$ is well controlled and typically takes a

value of around 0.3 for α_s values of relevance to low x physics in DIS.

Detailed data from HERA on power law fits are shown in figure 1.2. Figure 1.2(left) corresponds to inclusive data. The data exhibit clear transitions from a relatively soft energy dependence at low scales Q^2 to a stronger dependence at larger scales. As these more precise data emerged and were interpreted in more detail and subjected to fits to extract proton PDFs, it became well understood that a slowly rising behaviour at low Q^2 naturally changes into a faster-rising behaviour with increasing Q^2 through standard DGLAP evolution. This conclusion was further refined with increasingly precise HERA data over many years [Klein and Yoshida (2008)], culminating in the final combined H1 and ZEUS inclusive DIS measurements and their detailed interpretation in terms of proton structure [Abramowicz *et al.* (2015)].

Although the truly elastic $\gamma^* p$ cross section is not directly accessible experimentally, HERA provided extensive data [Newman and Wing (2014)] on exclusive vector meson production $\gamma^{(*)} p \to V p$ for real and virtual photons, with vector meson species including $V = \rho, \phi, J/\psi, \psi(2S)$ and Υ. These processes can be interpreted in terms of the elastic scattering of a $q\bar{q}$ dipole produced from a photon splitting, with subsequent formation of the vector meson. The closely related Deeply Virtual Compton Scattering process (DVCS, $\gamma^{(*)} p \to \gamma p$) was also studied [Aaron *et al.* (2008, 2009); Chekanov *et al.* (2009a)]. All of the measurements conformed to power law W dependences, with an effective pomeron intercept that evolved with scale from a soft behaviour e.g. in ρ photoproduction to a much harder value where large Q^2 or vector meson mass scales were extant. This tendency is illustrated for the photoproduction $Q^2 \to 0$ limit in figure 1.2(right). It is also clearly observed as Q^2 increases in ρ electroproduction data [Chekanov *et al.* (2007a); Aaron *et al.* (2010)].

Following the development of a framework [Bonvini *et al.* (2016)] to incorporate $\ln 1/x$ resummation [Altarelli *et al.* (2000, 2002)] at NLL accuracy, it became possible to include BFKL effects in otherwise standard DGLAP fits to inclusive ep data. A highly revealing fit to HERA data came from the recent study in the NNPDF framework [Forte *et al.* (2002)], including next-to-next-lo-leading order (NNLO) DGLAP evolution with NLL $\ln 1/x$ resummation [Ball *et al.* (2018)]. The substantial improvement in quality of fit to the data in [Abramowicz *et al.* (2015)] when the BFKL contribution is included originates from the small x, small Q^2 kinematic region, providing perhaps the most compelling evidence for BFKL dynamics in HERA data.

The interpretation of the novel effects that seem to be present in the lowest x HERA data is complicated by successful alternative descriptions, in which the $\gamma^* p$ cross section contains a low x saturation behaviour [Golec-Biernat and Wusthoff (1998)], which in the perturbative region might be interpreted as the onset of gluon recombination effects [Mueller (1990)]. This approach, based on density-driven low x effects in contrast to the energy-driven effects of BFKL, is usually implemented

in dipole models, which can be applied deep into the non-perturbative Q^2 region. The full story of low x physics at HERA is thus rather complicated and uncertain, possibly including a delicate interplay of effects which may not be fully describable with any single approximation to QCD. A fully detailed interpretation will surely not be possible without data from a future higher energy ep facility.

1.4 Inclusive Measurements

1.4.1 *Inclusive Measurements at VHEeP*

The VHEeP concept is very well suited to the study of inclusive cross sections at low x, since the centre of mass energies are the largest among current proposals and the low luminosity is not a major problem at modest Q^2. With the anticipated beam energies, values of W in the range $10^3 - 10^4$ GeV would be reachable, corresponding to x of $10^{-7} - 10^{-8}$ for $Q^2 = 1$ GeV^2.

Figure 1.3 [Caldwell and Wing (2016)] shows an initial study that illustrates the power of a machine such as VHEeP for the exploration of low x physics well beyond the kinematic region studied to date. Existing measurements of the inclusive neutral current ep cross section are shown in the form of the total $\gamma^* p$ cross section as a function of centre of mass energy W. Fits are shown for a range of scales Q^2 and two assumptions on the small x behavior. In one case, the cross section is assumed to continue to follow the simple power-law behavior $\sigma^{\gamma p} \propto x^{-\lambda(Q^2)}$ of figure 1.2a. In the second case, double asymptotic scaling predictions [Ball and Forte (1994)] are invoked, such that $\sigma^{\gamma p} \propto e^{B(Q^2)\sqrt{log(1/x)}}$. Whilst the HERA data are compatible with both of these assumptions, the curves diverge dramatically in the TeV energy range where VHEeP becomes sensitive. The double asymptotic scaling prediction is derived using DGLAP evolution assuming a soft input behaviour at small x, though other approaches including for example the BFKL resummation of [Ball *et al.* (2018)] or high density saturation [Golec-Biernat and Wusthoff (1998)] would have the same property of damping the growth with increasing W (or decreasing x) in the very high energy region, whilst maintaining an acceptable description of HERA data. If the luminosities achievable are sufficient to reach even a fraction of the Q^2 range shown, VHEeP would be an excellent facility to investigate the new low x effects implied by Lipatov's work in the context of inclusive data.

1.4.2 *Inclusive Measurements at LHeC and FCC-eh*

The physics capabilities of the LHeC ans FCC-eh concepts have been explored in considerable detail. The kinematic plane in (x, Q^2) for inclusive scattering is illustrated in figure 1.4, and placed in the context of other ep scattering facilities. Figure 1.4(left) shows the full kinematic plane, illustrating the extension towards lower x at fixed Q^2 by around an order of magnitude for LHeC over HERA and a further order of magnitude for FCC-eh. This gives the potential to approach

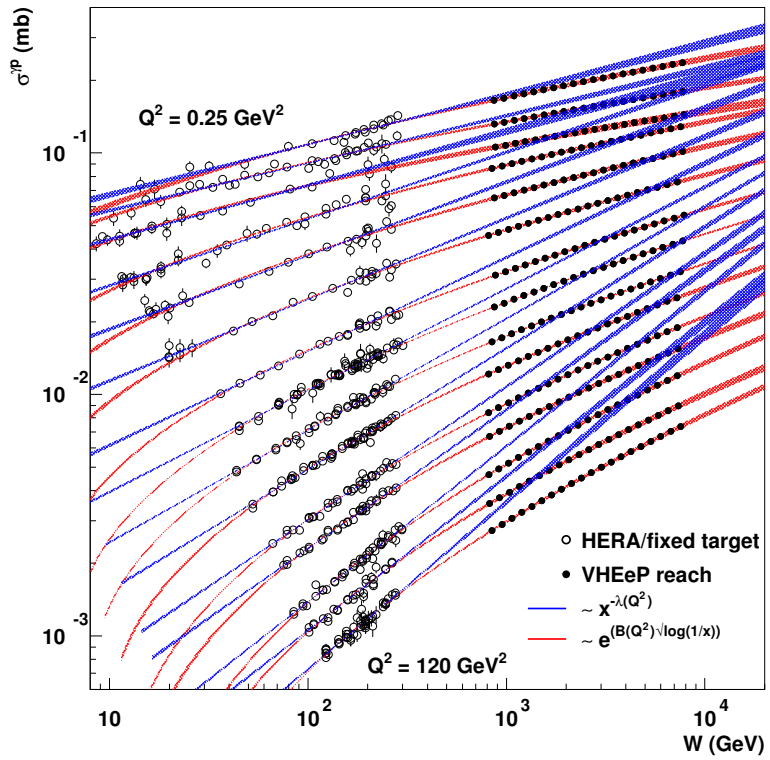

Fig. 1.3 Measurements (open points) of the total $\gamma^* p$ cross section as a function of centre of mass energy W for $0.25 < Q^2 < 120$ GeV^2 from HERA [Abramowicz *et al.* (2015)] and fixed-target experiments [Adams *et al.* (1996); Arneodo *et al.* (1997)]. The blue and red lines show different fits to the data as described in the text. The kinematic reach of VHEeP is illustrated by the closed points. The expected uncertainties per data point are yet to be evaluated, but at modest Q^2 thhey might be expected to reach the 1% level achieved at HERA. Figure taken from [Caldwell and Wing (2016)].

$x \sim 10^{-6}$ and $x \sim 10^{-7}$ at LHeC and FCC-eh, respectively, whilst remaining in the perturbative ($Q^2 > 1$ GeV^2) regime, a highly attractive perspective for investigating low x effects. The EIC is also shown in this figure. It has a role to play in bridging the gap between HERA and the fixed target facilities and providing information from a single facility in the high x region, potentially without complications from nuclear binding effects.

Figure 1.4(right) illustrates the importance, in the LHeC context, of ensuring that the detector acceptance for the scattered electron extends as close to the beamline as possible. A zoom is shown of the low x, low Q^2 corner of the kinematic plane ($x < 10^{-3}$), with lines of constant scattered electron angle superimposed. If the instrumentation required to detect and reconstruct the scattered electron stops at 10° from the beamline, only a small fraction of the low x corner of the kinematic

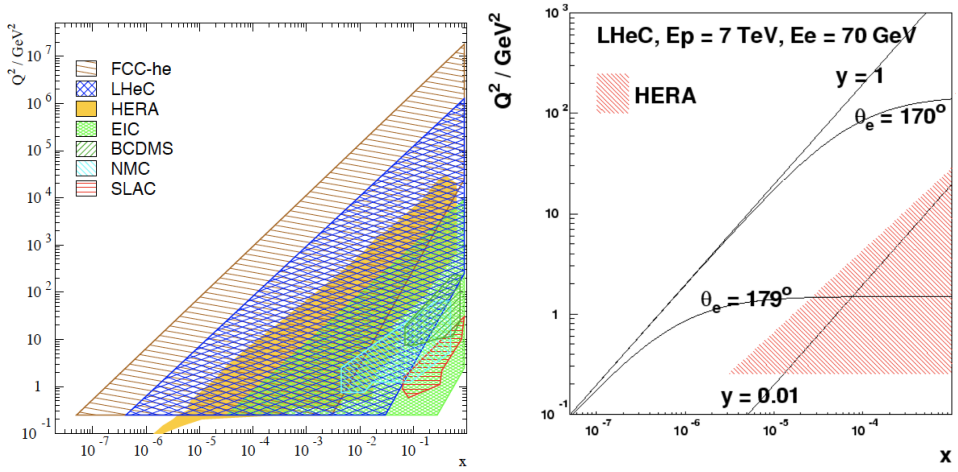

Fig. 1.4 (left) Kinematic plane showing acceptances as a function of x and Q^2 for various past and future DIS facilities, from [LHeC Study Group (2020)]. (right) Zoomed version of the kinematic plane for kinematics similar to those of the LHeC, restricted to $x < 10^{-3}$, from [Abelleira Fernandez *et al.* (2012)]. Lines of constant electron scattering angle $\theta_e = 1°$ and $10°$ are indicated, as is the approximate coverage of HERA.

plane, mostly with $Q^2 > 100$ GeV^2, is accessible. On the other hand, if scattered electrons can be efficiently and precisely reconstructed to within 1° to the beamline, the full kinematic plane with $Q^2 > 1$ GeV^2 becomes accessible, including the lowest x values. The need for near-hermetic acceptance, in the forward as well as the backward direction, is a recurring theme in LHeC physics.

One way to illustrate the power of the LHeC to constrain low x physics is by quantifying the improvements in precision on PDFs that it makes possible, assuming (bravely!) that $\ln 1/x$ effects can be ignored and that standard collinear evolution techniques remain applicable. In order to study this, LHeC 'pseudodata' are produced, simulating the sort of measurement that could be be made in terms of kinematic range and statistical and systematic precision. An integrated luminosity of 1 ab^{-1} is considered, though the results, especially for the low x region, are hardly affected if the 'LHeC first run' luminosity of 50 fb^{-1} is assumed instead. The pseudodata are included along with existing data in NLO and NNLO DGLAP-based fits, in the xFitter [Alekhin *et al.* (2015)] framework in a fitting procedure similar to that of HERAPDF2.0 [Abramowicz *et al.* (2015)]. One example result from this approach is shown in figure 1.5 [LHeC Study Group (2020)]. The current knowledge of the low x gluon density at a typical starting scale for DGLAP evolution in the fits ($Q^2 = 1.9$ GeV^2) is shown via error bands from various groups. Taking the error band from the NNPDF study suggests that there is some current knowledge of the gluon density down to $x \sim 10^{-4}$. However, when comparing with other fit results, there are differences between approaches for all values below $x \sim 10^{-3}$ despite them

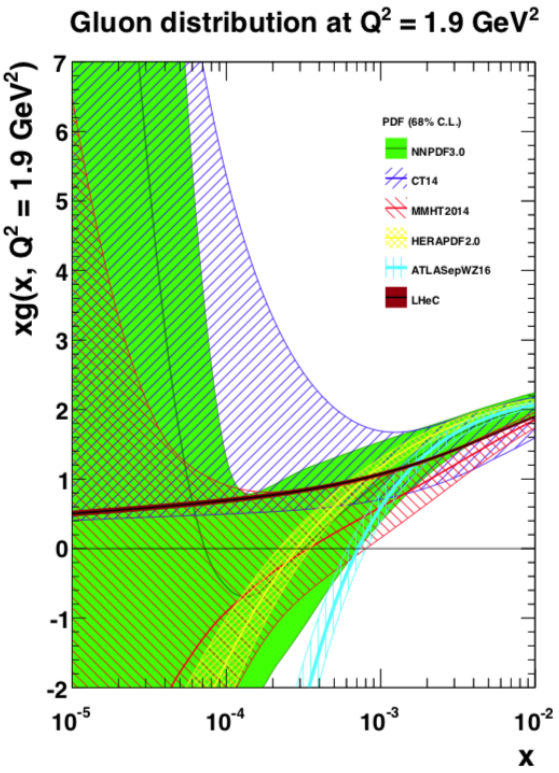

Fig. 1.5 Results of various NLO DGLAP QCD fits to extract the gluon density of the proton, shown in the form of uncertainty bands as a function of x at a scale $Q^2 = 1.9$ GeV^2. The global fits NNPDF3.0 [Ball *et al.* (2015)], CT14 [Dulat *et al.* (2016)] and MMHT2014 [Harland-Lang *et al.* (2015)] are shown, as well as fits that use HERA data only (HERAPDF2.0 [Abramowicz *et al.* (2015)]) and HERA plus selected LHC data (ATLASSepWZ16 [Aaboud *et al.* (2017)]). The brown band labelled LHeC shows the precision achieved when LHeC pseudodata are included in addition to HERA data, as described in detail in [LHeC Study Group (2020)].

having similar input data. The error bars also allow the possibility of a negative gluon density, with associated conceptual difficulties. In contrast, the fit in which LHeC pseudodata are included in addition to HERA data retains high precision on the gluon density throughout the region shown ($x > 10^{-5}$). As described in more detail in [LHeC Study Group (2020)], the relative precision obtained in the fits to including LHeC pseudodata is typically at the 1% on the gluon density down to $x = 10^{-5}$, with a further order of magnitude extension at FCC-eh. A full flavour decomposition for the quarks is also obtained at similar levels of precision. It is worth noting in passing that the projected impact of the 'ultimate' LHC pp data has also been investigated. Whilst the HL-LHC has some impact at intermediate and large x [Abdul Khalek *et al.* (2018)], it doesn't extend into the low x region of

interest here.

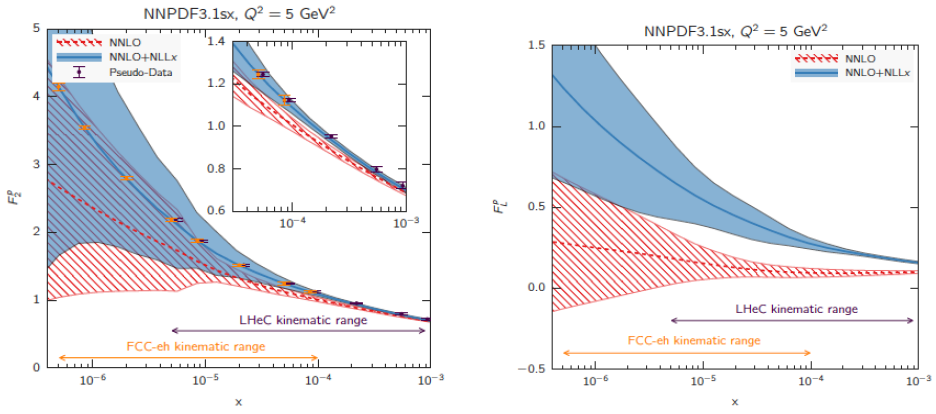

Fig. 1.6 Extrapolations of predictions for F_2 (left) and F_L (right) at $Q^2 = 5$ GeV^2 according to fits to HERA data in the NNPDF framework both with ('NNLO + NLLx') and without ('NNLO') including NLL BFKL $\ln 1/x$ resummation in the framework of [Bonvini *et al.* (2016)]. The error bands reflect the uncertainties on the basis of currently available data from HERA. The kinematic coverages at the LHeC and FCC-eh are indicated. The data points in the insert for F_2 show selected LHeC pseudodata [LHeC Study Group (2020)]. Figures taken from [Ball *et al.* (2018)].

The studies of PDF precision in the context of NLO or NNLO DGLAP QCD fits show that the LHeC offers a transformational level of precision at low x. However, it is also important to establish whether the kinematic region of sensitivity is sufficient to fully reveal and establish BFKL effects. This question is addressed in figures 1.6 and 1.7 [Ball *et al.* (2018)]. In figure 1.6 predictions for both of the inclusive DIS structure functions[3] F_2 and F_L are shown in the LHeC and FCC-eh kinematic regions based on extrapolations of the fits to HERA data with and without additional $\ln 1/x$ effects implemented through the HELL package [Bonvini *et al.* (2016)] (see section 1.3). The large uncertainty bands are simply a consequence of the lack of current constaints in the low x region beyond the sensitivity of HERA. Whilst the impact of the BFKL terms is subtle in HERA data, only being visible from careful consideration of the change in the χ^2 with the inclusion or removal of selected low x, low Q^2 data points, the effects become much more dramatic in the new low x region opened up by the proposed machines, as can be inferred from comparisons of the central values of the predictions. Due to its close relationship to the gluon density, the impact of including the NLL $\ln 1/x$ resummation is particularly pronounced for the structure function F_L, reaching a factor of four at $x = 10^{-6}$. As described in [LHeC Study Group (2020)], F_L can be measured at small x at the 10% level of precision at the LHeC from the change in the cross section at fixed x and Q^2 while $\sqrt{s}$ varies by taking data at three electron beam energies. Further immprovements

[3] See e.g. [Abramowicz *et al.* (2015)] for full formal definitions.

are possible at FCC-eh. Figure 1.6(right) suggests that such a precision is comfortably sufficient to identify and characterise low x effects beyond NNLO DGLAP. As can be seen in figure 1.6(left), the differences between the predictions for F_2 with and without $\ln 1/x$ resummation are also substantial, and much larger than the expected 1% level of experimental precision.

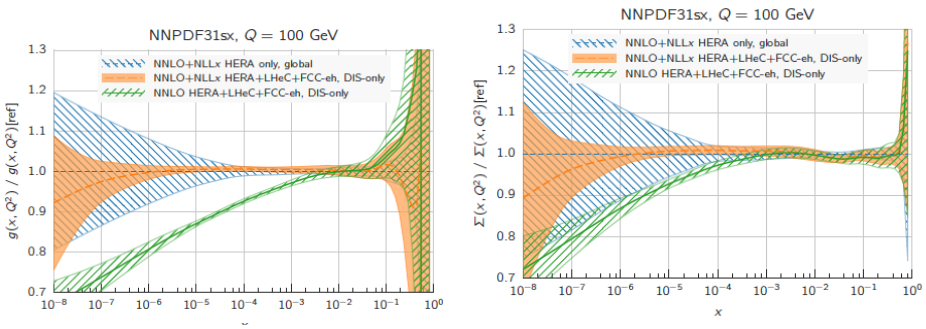

Fig. 1.7 Gluon (left) and singlet quark (right) distributions obtained in fits in the NNPDF framework relative to that in NNPDF3.1 [Ball *et al.* (2015)] at a scale of $Q^2 = 10^4$ GeV^2, extending to very low x. The error bands show the relative precision obtained when including only HERA data in the fit, or when additionally including LHeC and FCC-eh pseudodata, as indicated in the key. The central values correspond to fits in which no BFKL resummation is included ('NNLO') or in which NLL resummation is included in the framework of [Bonvini *et al.* (2016)] ('NNLO + NLLx'). The kinematic coverages at the LHeC and FCC-eh are indicated. Figures taken from [Ball *et al.* (2018)].

The comparisons in figure 1.6 have been developed further to investigate the impact of $\ln 1/x$ resummation on the proton parton densities in the LHeC and FCC-eh kinematic range. Figure 1.7 shows the gluon and singlet quark distributions at an example $Q^2 = 10^4$ GeV^2 as a function of x relative to a reference provided by the NNPDF 3.1 extrapolation to very low x including the NLL BFKL resummation. Comparison of the error bands for the 'NNLO + NLLx' predictions with and without pseudodata from the new proposed colliders illustrates once again that the sensitivity of LHeC and FCC-eh extends to around $x = 10^{-6} - 10^{-7}$. Comparison of the central values for 'NNLO + NLLx' and 'NNLO' illustrates the large effect of including BFKL effects on the extracted parton densities The size of the BFKL effect is slightly larger for the gluon density than for the quarks, reaching almost 30% at $x = 10^{-7}$.

1.5 Exclusive and Semi-inclusive Measurements

1.5.1 *Exclusive Vector Meson Production*

The lowest order underlying parton level process leading to the quasi-elastic, or exclusive, production of vector mesons is illustrated in figure 1.8(left). As discussed

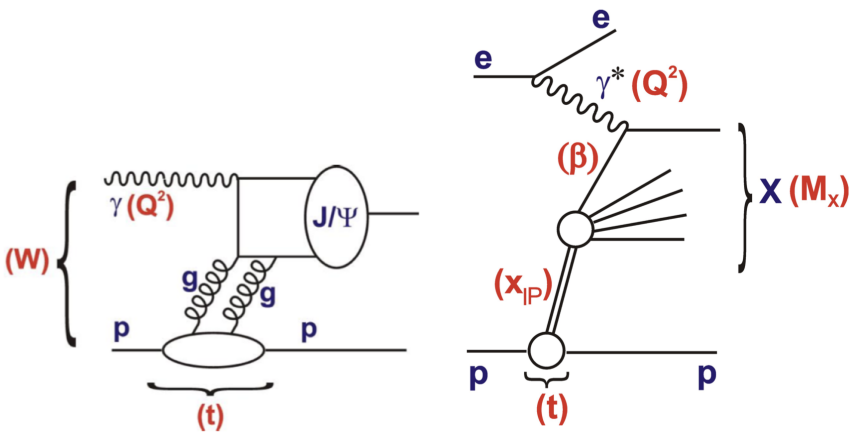

Fig. 1.8 Illustration of diffractive processes in ep scattering and the kinematic variables used to describe them. (left) Lowest order QCD diagram for exclusive or 'quasi-elastic' J/ψ photoproduction ($\gamma p \to J/\psi p$), where the incoming photon couples to the electron. (right) Inclusive diffractive deep inelastic scattering ($ep \to eXp$), shown mediated by a generic pomeron.

in section 1.3, the predicted cross section follows a power law $\mathrm{d}\sigma_{\mathrm{el}}/\mathrm{d}t \propto s^{2\alpha(0)-2}$ at vanishing t and if the two gluon exchange shown is replaced by the full BFKL pomeron, $\alpha(0) = 1 + \omega_{I\!P}$.

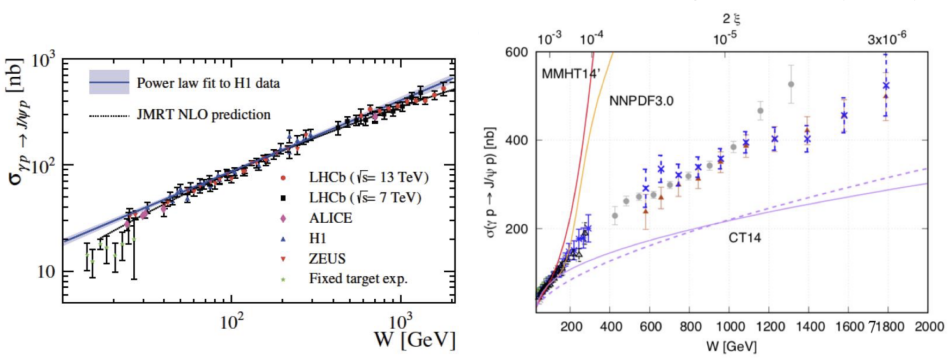

Fig. 1.9 (left) Current data on the total cross section for quasi-elastic J/ψ photoproduction ($\gamma p \to J/\psi p$) as a function of γp centre of mass energy, including measurements from H1 [Alexa *et al.* (2013); Aktas *et al.* (2006a)] and ZEUS [Chekanov *et al.* (2002)] at HERA, as well as ALICE [Abelev *et al.* (2014)] and LHCb [Aaij *et al.* (2014, 2018)] at the LHC (figure from [Aaij *et al.* (2018)]). (right) HERA J/ψ photoproduction data compared with predictions from a k_T factorisation model [Flett *et al.* (2019)] assuming different input gluon distributions [Harland-Lang *et al.* (2015); Dulat *et al.* (2016); Ball *et al.* (2015)].

Among the possible vector meson studies, J/ψ photoproduction has perhaps a special role. In models built using QCD starting from the low x gluon density

[Martin *et al.* (1997)], the relevant scale of $\bar{Q}^2 = (Q^2 + M_V^2)/4 \sim 3$ GeV^2 lies in the perturbative domain, whilst effective x values $\bar{x} = (Q^2 + M_V^2)/(Q^2 + W^2)$ as low as 10^{-5} are probed at the LHeC, with further extensions towards lower x at FCC-eh and VHEeP. As well as being studied in detail at HERA, this process has been the subject of substantial investigation in ultra-peripheral collisions at the LHC, where an incoming proton or lead ion provides the source of photons in place of the electron at HERA. As shown in figure 1.9(left), the LHC measurements[4] confirm the HERA power law energy dependence and, particularly for the favourable forward acceptance of LHCb, extend the kinematic range to higher W. The energy dependence of the J/ψ production process is fully compatible with a power law behaviour and corresponds to $\alpha(\langle t \rangle) \simeq 1.2$ when averaged over t. It has been interpreted starting from a knowledge of the proton gluon density by a number of groups [Martin *et al.* (2000); Frankfurt *et al.* (2001); Martin *et al.* (2008)] with the conclusion that the data can be described using the gluon density extracted from inclusive DIS, but with scale uncertainties that are hard to control. A recent approach [Flett *et al.* (2019)] attempts to tackle these issues in the framework of k_T factorisation. As shown in figure 1.9(right), in this approach the J/ψ data potentially powerfully distinguish between different proton PDF sets. From an alternative viewpoint, this strong variation of the predictions with input PDF set suggests that unintegrated gluons may ultimately be the appropriate building blocks for the study of low x final states including vector meson production.

Independently of the detailed conclusions from HERA and LHC data, it is clear that high energy exclusive vector meson photoproduction and leptoproduction data may play a crucial role in our future understanding of low x physics. They are therefore an important target for the future ep facilities currently under discussion. The limited centre of mass reach of the EIC and its ability to polarise both beams imply that its vector meson and DVCS programme will focus on spatial imaging, correlations and spin structure [Aschenauer *et al.* (2019)] rather than on low x aspects. The potential ultra-low-x reach of the VHEeP facility has exciting potential and the low luminosities should not be a strong impediment to the study of at least ρ, ϕ and J/ψ production. However detailed studies have yet to be carried out. On the other hand, the LHeC's capabilities have been investigated in some detail, in particular for J/ψ photoproduction. As shown in figure 1.10(left), a very precise measuerment is possible in the decay channel $J/\psi \to \mu^+\mu^-$ with a modest luminosity of 2 fb^{-1}, provided the muon detector acceptance extends to within 1° of the beamline. Whilst the W range is a substantial improvement over that available at HERA, it does not extend beyond the upper limits reached by LHCb. However, the power of a future ep machine may lie more in well controlled proton tagging and precise transverse momentum meassurements, for example using the Roman pot technique that was already successfully applied at HERA [Aaron *et al.* (2012a)].

[4]The CMS collaboration has made similar measurements for exclusive ρ [Sirunyan *et al.* (2019a)] and Υ [Sirunyan *et al.* (2019b)] meson production.

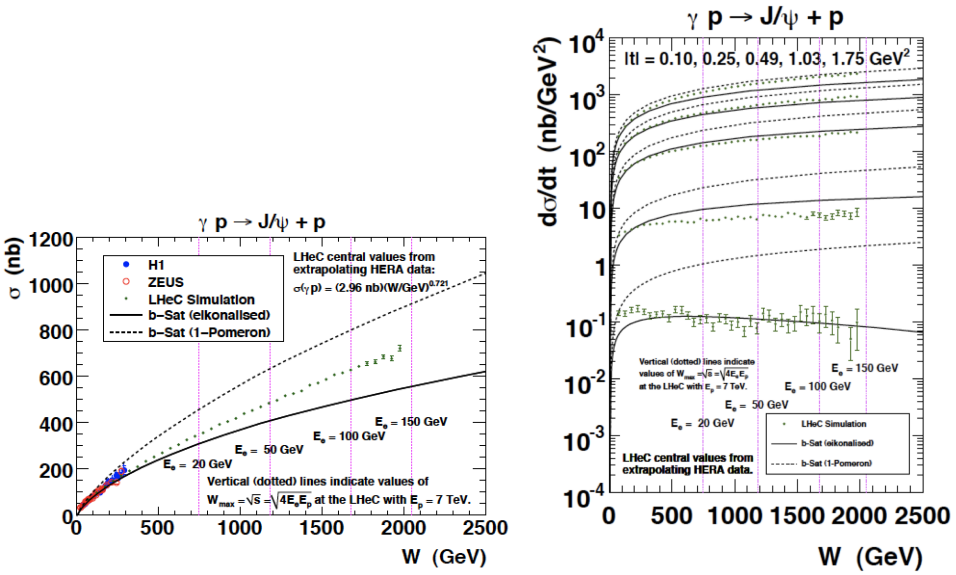

Fig. 1.10 Pseudodata based on LHeC kinematics for quasi-elastic J/ψ photoproduction ($\gamma p \to J/\psi p$). The cross section is shown as a function of W in the left panel, whilst the right panel shows W dependences differentially in t at the t values indicated, running from top to bottom. Limits imposed by different electron beam energies are indicated. An integrated luminosity of 2 fb^{-1} is assumed. The full and dotted lines correspond to two different versions of the b-Sat dipole model [Kowalski *et al.* (2006)], in which low x density-driven saturation is included as a function of impact parameter ('eikonalised'), or is omitted ('1 pomeron'). The data shown in the left panel are taken from HERA [Aktas *et al.* (2006a); Chekanov *et al.* (2002)]. The figures are taken from [Abelleira Fernandez *et al.* (2012)].

This becomes clear from simulations of differential measurements as a function of W and t, as shown in figure 1.10(right). The delicate interplay between energy-driven BFKL effects and density driven saturation effects will require this sort of detail, and possibly the additional inclusion of coherent vector meson production from nuclei $eA \to eVA$, as explored further in [LHeC Study Group (2020)].

Although not yet studied in the context of the proposed high energy colliders, it is worth noting that quasi-elastic processes at very large $|t|$ offer a highly promising environment in which to search for BFKL effects. The large $|t|$ ensures that the exchange is genuinely hard, whilst still satisfying the Regge limit $s \gg |t|$. One such process is the production of large rapidity gaps between high transverse momentum jets in photoproduction, where the HERA data [Adloff *et al.* (2002); Chekanov *et al.* (2007b)] have been compared with leading log BFKL calculations [Mueller and Tang (1992); Enberg *et al.* (2002)] with some degree of success, the achievable precision being limited by the poorly constrained rapidity gap survival probability. A related process is diffractive vector meson (particularly J/ψ) production at large $|t|$, where again the data [Aktas *et al.* (2003); Chekanov *et al.* (2010)] and BFKL-

based predictions [Forshaw and Ryskin (1995); Bartels *et al.* (1996b); Forshaw and Poludniowski (2003)] are broadly in agreement. Whilst the calculations are not yet at a stage where they can accurately reproduce the data, the shere existence of such processes is highly suggestive of the presence of BFKL dynamics and further high luminosity data at the LHeC, FCC-eh or VHEeP could have a major impact.

1.5.2 *Inclusive Diffractive DIS*

The inclusive diffractive process in DIS ($ep \to eXp$) is illustrated in figure 1.8(right). The proton remains intact, tranferring a fraction $x_{I\!P} \equiv \xi$ of its longitudinal momentum through a colourless exchange to create a multi-particle system X with a continuous mass distribution that can be viewed as the products of the dissociation of the virtual photon, correspondingly with overall 1^{--} quantum numbers. The fraction of the proton longitudinal momentum loss that is carried by the struck quark is denoted β, such that $\beta x_{I\!P} = x$. One important observation from HERA was that this DDIS process comprises a large ($\sim 10\,\%$) fraction of diffractive events, to first approximation independently of Q^2 [Derrick *et al.* (1993b); Ahmed *et al.* (1994)]. In a long series of papers (see [Newman and Wing (2014)] for a review), the HERA experiments determined the deep inelastic structure of the t-channel exchange in these events in the form of diffractive parton densities, as well as studying the energy dependence in the form of the variation with $x_{I\!P}$ at fixed β and Q^2. The diffractive parton densities are often interpreted [Ingelman and Schlein (1985)] in terms of a structure for the pomeron. They were found to be strongly gluon dominated, encouraging interpretations in which DDIS is closely related to the gluon dynamics also discussed in the inclusive case. Interestingly, the final results from HERA on the effective pomeron intercept describing DDIS are well aligned at around $\alpha(0) \sim 1.12^{+0.03}_{-0.01}$ [Aktas *et al.* (2006c); Chekanov *et al.* (2009b); Aaron *et al.* (2012b)], more compatible with a soft pomeron than a BFKL pomeron, so the picture for the dominant process is more one of the virtual photon probing a soft pomeron exchange than of the progressively harder processes that are observed at large scales in the vecor meson case (section 1.5.1). The picture is therefore a rather complex one, whose thorough understanding requires the study of DDIS at future higher energy ep colliders. Mapping in detail the evolution with energy has considerable promise to unravel the delicate interplay between higher twist effects at low Q^2, the onset of BFKL effects at low β or x and eventually non-linear dynamics at high densities.

An investigation of the potential studies of inclusive diffraction that would be possible at the EIC and LHeC is presented in [Armesto *et al.* (2019)]. Although that work is performed at NLO, similar analyses in the HERA context have recently been extended to NNLO [Khanpour (2019)]. In figure 1.11, the accessible kinematic range in (x, Q^2) is shown for HERA, EIC, LHeC and FCC-eh. For the LHeC design the range in x is increased by a factor ~ 20 over HERA and the maximum available Q^2 by a factor ~ 100. The FCC-eh machine would further increase this

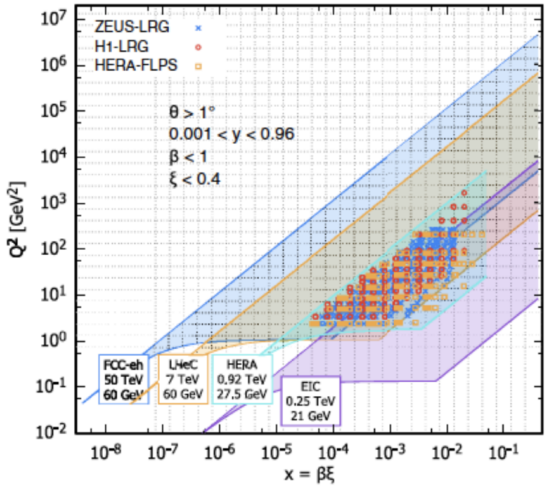

Fig. 1.11 Kinematic plane indicating the acceptance for inclusive diffraction in (x, Q^2) for the EIC (magenta region), the LHeC (orange region) and the FCC-eh (dark blue region) as compared with the HERA data (light blue region, [Chekanov *et al.* (2009b); Aaron *et al.* (2012b,a)]). The acceptance limit for the scattered electron is assumed to be 1°, and ξ values up to 0.4 are included. Figure taken from [Armesto *et al.* (2019)].

range by roughly one order of magnitude in both x and Q^2. The EIC coverage is complementary, adding sensitivity at higher x than HERA, a region which is currently unexplored due to the lack of DDIS measurements in fixed target ep scattering experiments. The LHeC (FCC-eh) machine probes very small values of ξ, reaching 10^{-4} (10^{-5}) for $\beta \sim 10^{-2}$. At $\xi = 0.1$, the LHeC and FCC-eh kinematic ranges extend down to $\beta \sim 10^{-5}$ and $\beta \sim 10^{-6}$, respectively, offering the enticing prospect of studying diffractive DIS in a wider β, Q^2 kinematic range than has been possible in (x, Q^2) for inclusive DIS at HERA. These kinematic coverages are clearly very well suited to the study of new low x effects.

Based on the studies in [Armesto *et al.* (2019)], the experimental precision with which the diffractive gluon density could be extracted when LHeC and FCC-eh data become available is illustated in figure 1.12. The predicted fractional uncertainties are shown for the LHeC and FCC-eh at two different scales Q^2 as a function of parton momentum fraction z. The different bands show the variation with the upper cut on the available ξ range, from 0.01 to 0.32. In the best constrained region of $z \simeq 0.1$, the precision reaches the 1% level, with only a small dependence on the available ξ range. The low x DPDF determination accuracy improves with respect to HERA by a factor of 5–7 for the LHeC and 10–15 for the FCC-eh and completely new kinematic regimes are accessed.

The hadronic final state in DDIS may offer further insights into low x effects. For example, diffractive charm production [Aktas *et al.* (2007); Chekanov *et al.* (2003)]

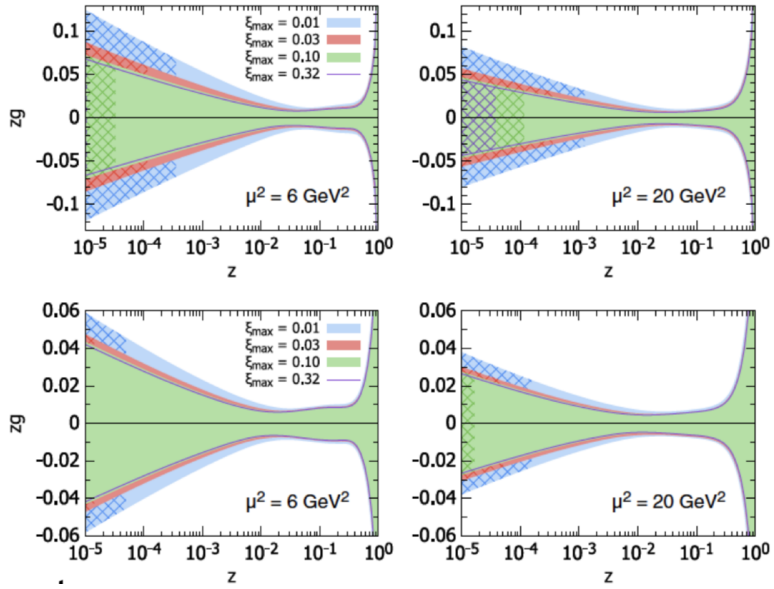

Fig. 1.12 Relative experimental uncertainties on the diffractive gluon density for LHeC kinematics (upper panel) and FCC-eh kinematics (lower panel). Two different choices of scale, $\mu^2 = 6$ and 20 GeV^2, are considered. The blue, red and green bands and the magenta line correspond to different maximal values of $\xi = 0.01, 0.03, 0.1, 0.32$, respectively. The cross-hatched areas show regions which are not directly accessible in data and require extrapolations. Theoretical uncertainties, for example due to parameterisation bias or variations in scales and heavy quark masses, are not included. Figure taken from [Armesto *et al.* (2019)].

has been successfully modelled in terms of a gluon pair or ladder coupling to a basic $\gamma^* \to q\bar{q}$ or $\gamma^* \to q\bar{q}g$ fluctuation, using k_T factorisation and an unintegrated gluon density in the 'BJKLW' model [Bartels *et al.* (1996c,a, 1999, 2002)]. The prospects at future facilities have yet to be explored in detail. The much larger photon dissociation masses that become accessible kinematically at the LHeC or FCC-eh offer the interesting possibility of accessing very low z values, though this region also enhances the $q\bar{q}g$ and higher multiplicity photon fluctuations that are difficult to handle theoretically.

1.6 Inclusive Hadronic Final State Measurements

Much of the search programme for BFKL effects in HERA data was focused on hadronic final state measurements. A large part of this work involved looking for deviations from the transverse momentum ordering of successively emitted partons along the parton cascade between the photon and the proton that is implied by DGLAP evolution. If BFKL effects are the dominant feature of the data, one expects instead to find strong x (or energy) ordering, as illustrated in figure 1.13(left).

Observables that are sensitive to these differences include azimuthal decorrelations between jets, Mueller-Navelet jet configurations and forward particle or energy flows, as summarised for example in [Jung, H. (2020)].

The potential to reveal BFKL effects in the hadronic final state has yet to be investigated in detail for future *ep* colliders, though clearly the enhanced reach towards low x will be a major benefit. A flavour of the potential to observe these effects is shown in figure 1.13(right). Following the approach in [Aktas *et al.* (2006b)], simulated cross sections are shown for forward jets in the range of angles relative to the outgoing proton direction $1^\circ < \theta < 20^\circ$, with transverse energy $E_T > 10$ GeV, as a function of Bjorken-x. The curve labelled 'MEPS' corresponds to a standard (RAPGAP [Jung (1995)]) Monte Carlo implmentation of LO matrix elements interfaced to DGLAP parton showers, implying transverse momentum ordering along the parton cascade. On the other hand, the 'CDM' curve is obtained from the DJANGO / ARIADNE programmes [Charchula *et al.* (1994); Lonnblad (1992)] and includes the BFKL-like feature of energy ordering. The CASCADE programme [Jung and Salam (2001); Jung (2002)] uses an unintegrated gluon density as input and implements the angular parton cascade ordering of the CCFM formalism [Ciafaloni (1988); Catani *et al.* (1990a,b); Marchesini (1995)], in which both $\ln 1/x$ and $\ln Q^2$ terms are resummed in the relevant limits. The CDM model predicts almost a factor of five enhancement of forward jet production over the other models. With LHeC energies and sufficiently forward instrumentation, observables such as forward jets thus appear likely to be highly powerful in distinguishing between different types of parton evolution dynamics and ultimately characterising the transition to a BFKL-dominated domain.

1.7 Conclusion

Lev Lipatov is unquestionably a giant of low x physics. Whilst his work already underlies a wide range of theoretical aspects of the field, the impact of his best-known contributions in the BFKL context only just start to be seen in experimental data, presumably due to the need for high energies to approach the rather ill-defined 'asymptotic' kinematic region. Here only a flavour has been given of the possible future directions of the subject. As we now look towards the development of new DIS facilities, with increased centre-of-mass energies a major theme, it is inevitable that Lipatov's legacy will become more and more apparent over the coming decades.

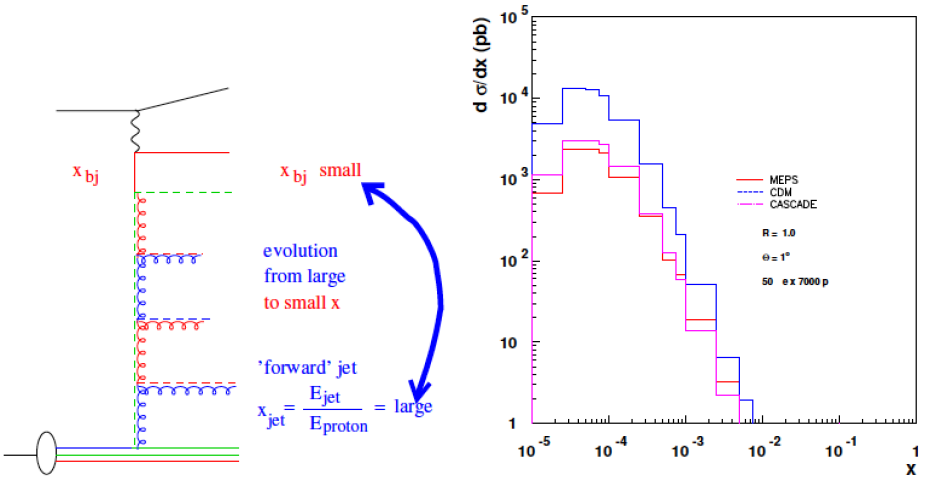

Fig. 1.13 (left) Illustration of a parton cascade in a low x ep process in which BFKL evolution dominates (the lengths of the emitted partons is representative of their energies). (right) Simulated cross sections for forward jet production wirth $E_T > 10$ GeV in the angular range $3 < \theta < 20°$ relative to the outgoing proton beam as a function of Bjorken x in the LHeC context. Jets are found using the SIScone algorithm [Salam and Soyez (2007)] with $R = 0.5$. The predictions of three Monte Carlo models with differening parton cascade dynamics as described in the text are compared. Figure taken from [Abelleira Fernandez *et al.* (2012)].

Bibliography

Aaboud, M. *et al.* (2017). Precision measurement and interpretation of inclusive W^+ , W^- and Z/γ^* production cross sections with the ATLAS detector, *Eur. Phys. J.* **C77**, 6, p. 367, doi:10.1140/epjc/s10052-017-4911-9, arXiv:1612.03016 [hep-ex].

Aaij, R. *et al.* (2014). Updated measurements of exclusive J/ψ and ψ(2S) production cross-sections in pp collisions at $\sqrt{s} = 7$ TeV, *J. Phys.* **G41**, p. 055002, doi:10.1088/0954-3899/41/5/055002, arXiv:1401.3288 [hep-ex].

Aaij, R. *et al.* (2018). Central exclusive production of J/ψ and $\psi(2S)$ mesons in pp collisions at $\sqrt{s} = 13$ TeV, *JHEP* **10**, p. 167, doi:10.1007/JHEP10(2018)167, arXiv:1806.04079 [hep-ex].

Aaron, F. D. *et al.* (2008). Measurement of deeply virtual Compton scattering and its t-dependence at HERA, *Phys. Lett.* **B659**, pp. 796–806, doi:10.1016/j.physletb.2007.11.093, arXiv:0709.4114 [hep-ex].

Aaron, F. D. *et al.* (2009). Deeply Virtual Compton Scattering and its Beam Charge Asymmetry in e+- Collisions at HERA, *Phys. Lett.* **B681**, pp. 391–399, doi:10.1016/j.physletb.2009.10.035, arXiv:0907.5289 [hep-ex].

Aaron, F. D. *et al.* (2010). Diffractive Electroproduction of rho and phi Mesons at HERA, *JHEP* **05**, p. 032, doi:10.1007/JHEP05(2010)032, arXiv:0910.5831 [hep-ex].

Aaron, F. D. *et al.* (2012a). Combined inclusive diffractive cross sections measured with forward proton spectrometers in deep inelastic ep scattering at HERA, *Eur. Phys. J.* **C72**, p. 2175, doi:10.1140/epjc/s10052-012-2175-y, arXiv:1207.4864 [hep-ex].

Aaron, F. D. *et al.* (2012b). Inclusive Measurement of Diffractive Deep-Inelastic Scattering at HERA, *Eur. Phys. J.* **C72**, p. 2074, doi:10.1140/epjc/s10052-012-2074-2, arXiv:1203.4495 [hep-ex].

Abada, A. *et al.* (2019). FCC Physics Opportunities, *Eur. Phys. J.* **C79**, 6, p. 474, doi:10.1140/epjc/s10052-019-6904-3.

Abdul Khalek, R., Bailey, S., Gao, J., Harland-Lang, L., and Rojo, J. (2018). Towards Ultimate Parton Distributions at the High-Luminosity LHC, *Eur. Phys. J.* **C78**, 11, p. 962, doi:10.1140/epjc/s10052-018-6448-y, arXiv:1810.03639 [hep-ph].

Abelev, B. B. *et al.* (2014). Exclusive J/ψ photoproduction off protons in ultra-peripheral p-Pb collisions at $\sqrt{s_{\rm NN}} = 5.02$ TeV, *Phys. Rev. Lett.* **113**, 23, p. 232504, doi:10.1103/PhysRevLett.113.232504, arXiv:1406.7819 [nucl-ex].

Abelleira Fernandez, J. L. *et al.* (2012). A Large Hadron Electron Collider at CERN: Report on the Physics and Design Concepts for Machine and Detector, *J. Phys.* **G39**, p. 075001, doi:10.1088/0954-3899/39/7/075001, arXiv:1206.2913 [physics.acc-ph].

Abramowicz, H. *et al.* (2015). Combination of measurements of inclusive deep inelastic $e^{\pm}p$ scattering cross sections and QCD analysis of HERA data, *Eur. Phys. J.* **C75**,

12, p. 580, doi:10.1140/epjc/s10052-015-3710-4, arXiv:1506.06042 [hep-ex].

Abt, I. *et al.* (1993). Measurement of the proton structure function F2 (x, Q**2) in the low x region at HERA, *Nucl. Phys.* **B407**, pp. 515–538, doi:10.1016/0550-3213(93)90090-C.

Accardi, A. *et al.* (2016). Electron Ion Collider: The Next QCD Frontier, *Eur. Phys. J.* **A52**, 9, p. 268, doi:10.1140/epja/i2016-16268-9, arXiv:1212.1701 [nucl-ex].

Adams, M. R. *et al.* (1996). Proton and deuteron structure functions in muon scattering at 470-GeV, *Phys. Rev.* **D54**, pp. 3006–3056, doi:10.1103/PhysRevD.54.3006.

Adloff, C. *et al.* (2002). Energy flow and rapidity gaps between jets in photoproduction at HERA, *Eur. Phys. J.* **C24**, pp. 517–527, doi:10.1007/s10052-002-0988-9, arXiv:hep-ex/0203011 [hep-ex].

Ahmed, T. *et al.* (1994). Deep inelastic scattering events with a large rapidity gap at HERA, *Nucl. Phys.* **B429**, pp. 477–502, doi:10.1016/0550-3213(94)90151-1.

Aktas, A. *et al.* (2003). Diffractive photoproduction of J/ψ mesons with large momentum transfer at HERA, *Phys. Lett.* **B568**, pp. 205–218, doi:10.1016/j.physletb.2003.06.056, arXiv:hep-ex/0306013 [hep-ex].

Aktas, A. *et al.* (2006a). Elastic J/psi production at HERA, *Eur. Phys. J.* **C46**, pp. 585–603, doi:10.1140/epjc/s2006-02519-5, arXiv:hep-ex/0510016 [hep-ex].

Aktas, A. *et al.* (2006b). Forward jet production in deep inelastic scattering at HERA, *Eur. Phys. J.* **C46**, pp. 27–42, doi:10.1140/epjc/s2005-02471-x, arXiv:hep-ex/0508055 [hep-ex].

Aktas, A. *et al.* (2006c). Measurement and QCD analysis of the diffractive deep-inelastic scattering cross-section at HERA, *Eur. Phys. J.* **C48**, pp. 715–748, doi:10.1140/epjc/s10052-006-0035-3, arXiv:hep-ex/0606004 [hep-ex].

Aktas, A. *et al.* (2007). Diffractive open charm production in deep-inelastic scattering and photoproduction at HERA, *Eur. Phys. J.* **C50**, pp. 1–20, doi:10.1140/epjc/s10052-006-0206-2, arXiv:hep-ex/0610076 [hep-ex].

Alekhin, S. *et al.* (2015). HERAFitter, *Eur. Phys. J.* **C75**, 7, p. 304, doi:10.1140/epjc/s10052-015-3480-z, arXiv:1410.4412 [hep-ph].

Alexa, C. *et al.* (2013). Elastic and Proton-Dissociative Photoproduction of J/psi Mesons at HERA, *Eur. Phys. J.* **C73**, 6, p. 2466, doi:10.1140/epjc/s10052-013-2466-y, arXiv:1304.5162 [hep-ex].

Altarelli, G., Ball, R. D., and Forte, S. (2000). Resummation of singlet parton evolution at small x, *Nucl. Phys.* **B575**, pp. 313–329, doi:10.1016/S0550-3213(00)00032-8, arXiv:hep-ph/9911273 [hep-ph].

Altarelli, G., Ball, R. D., and Forte, S. (2002). Factorization and resummation of small x scaling violations with running coupling, *Nucl. Phys.* **B621**, pp. 359–387, doi:10.1016/S0550-3213(01)00563-6, arXiv:hep-ph/0109178 [hep-ph].

Altarelli, G. and Parisi, G. (1977). Asymptotic Freedom in Parton Language, *Nucl. Phys.* **B126**, pp. 298–318, doi:10.1016/0550-3213(77)90384-4.

Angal-Kalinin, D. *et al.* (2018). PERLE. Powerful energy recovery linac for experiments. Conceptual design report, *J. Phys.* **G45**, 6, p. 065003, doi:10.1088/1361-6471/aaa171, arXiv:1705.08783 [physics.acc-ph].

Armesto, N., Newman, P. R., Słomiński, W., and Staśto, A. M. (2019). Inclusive diffraction in future electron-proton and electron-ion colliders, *Phys. Rev.* **D100**, 7, p. 074022, doi:10.1103/PhysRevD.100.074022, arXiv:1901.09076 [hep-ph].

Arneodo, M. *et al.* (1997). Measurement of the proton and deuteron structure functions, F2(p) and F2(d), and of the ratio sigma-L / sigma-T, *Nucl. Phys.* **B483**, pp. 3–43, doi:10.1016/S0550-3213(96)00538-X, arXiv:hep-ph/9610231 [hep-ph].

Aschenauer, E. C., Fazio, S., Lee, J. H., Mantysaari, H., Page, B. S., Schenke, B., Ullrich,

T., Venugopalan, R., and Zurita, P. (2019). The electron–ion collider: assessing the energy dependence of key measurements, *Rept. Prog. Phys.* **82**, 2, p. 024301, doi:10.1088/1361-6633/aaf216, arXiv:1708.01527 [nucl-ex].

Balitsky, I. I. and Lipatov, L. N. (1978). The Pomeranchuk Singularity in Quantum Chromodynamics, *Sov. J. Nucl. Phys.* **28**, pp. 822–829, [Yad. Fiz.28,1597(1978)].

Ball, R. D., Bertone, V., Bonvini, M., Marzani, S., Rojo, J., and Rottoli, L. (2018). Parton distributions with small-x resummation: evidence for BFKL dynamics in HERA data, *Eur. Phys. J.* **C78**, 4, p. 321, doi:10.1140/epjc/s10052-018-5774-4, arXiv:1710.05935 [hep-ph].

Ball, R. D. and Forte, S. (1994). Double asymptotic scaling at HERA, *Phys. Lett.* **B335**, pp. 77–86, doi:10.1016/0370-2693(94)91561-X, arXiv:hep-ph/9405320 [hep-ph].

Ball, R. D. *et al.* (2015). Parton distributions for the LHC Run II, *JHEP* **04**, p. 040, doi:10.1007/JHEP04(2015)040, arXiv:1410.8849 [hep-ph].

Bartels, J., Ewerz, C., Lotter, H., and Wusthoff, M. (1996a). Azimuthal distribution of quark - anti-quark jets in DIS diffractive dissociation, *Phys. Lett.* **B386**, pp. 389–396, doi:10.1016/0370-2693(96)81071-9, arXiv:hep-ph/9605356 [hep-ph].

Bartels, J., Forshaw, J. R., Lotter, H., and Wusthoff, M. (1996b). Diffractive production of vector mesons at large t, *Phys. Lett.* **B375**, pp. 301–309, doi:10.1016/0370-2693(96)00203-1, arXiv:hep-ph/9601201 [hep-ph].

Bartels, J., Jung, H., and Kyrieleis, A. (2002). Massive c anti-c g: Calculation in diffractive DIS and diffractive D* production at HERA, *Eur. Phys. J.* **C24**, pp. 555–560, doi:10.1007/s10052-002-0991-1, arXiv:hep-ph/0204269 [hep-ph].

Bartels, J., Jung, H., and Wusthoff, M. (1999). Quark - anti-quark gluon jets in DIS diffractive dissociation, *Eur. Phys. J.* **C11**, pp. 111–125, doi:10.1007/s100520050618,10.1007/s100529900081, arXiv:hep-ph/9903265 [hep-ph].

Bartels, J., Lotter, H., and Wüsthoff, M. (1996c). Quark-antiquark production in DIS diffractive dissociation, *Phys. Lett.* **B379**, pp. 239–248, doi:10.1016/0370-2693(96)00412-1,10.1016/0370-2693(96)00840-4, arXiv:hep-ph/9602363 [hep-ph], [Erratum: Phys. Lett.B382,449(1996)].

Bonvini, M., Marzani, S., and Peraro, T. (2016). Small-x resummation from HELL, *Eur. Phys. J.* **C76**, 11, p. 597, doi:10.1140/epjc/s10052-016-4445-6, arXiv:1607.02153 [hep-ph].

Caldwell, A., Ent, R., Levy, A., Newman, P., and Olness, F. (2018). The "DIS and Related Subjects" Strategy Document: Fundamental Science from Lepton-Hadron Scattering, arXiv:1812.08110 [hep-ph].

Caldwell, A. and Wing, M. (2016). VHEeP: A very high energy electron–proton collider, *Eur. Phys. J.* **C76**, 8, p. 463, doi:10.1140/epjc/s10052-016-4316-1, arXiv:1606.00783 [hep-ex].

Catani, S., Ciafaloni, M., and Hautmann, F. (1991). High-energy factorization and small x heavy flavor production, *Nucl. Phys.* **B366**, pp. 135–188, doi:10.1016/0550-3213(91)90055-3.

Catani, S., Fiorani, F., and Marchesini, G. (1990a). QCD Coherence in Initial State Radiation, *Phys. Lett.* **B234**, pp. 339–345, doi:10.1016/0370-2693(90)91938-8.

Catani, S., Fiorani, F., and Marchesini, G. (1990b). Small x Behavior of Initial State Radiation in Perturbative QCD, *Nucl. Phys.* **B336**, pp. 18–85, doi:10.1016/0550-3213(90)90342-B.

Charchula, K., Schuler, G. A., and Spiesberger, H. (1994). Combined QED and QCD radiative effects in deep inelastic lepton - proton scattering: The Monte Carlo generator DJANGO6, *Comput. Phys. Commun.* **81**, pp. 381–402, doi:10.1016/0010-4655(94)90086-8.

Chekanov, S. *et al.* (2002). Exclusive photoproduction of J / psi mesons at HERA, *Eur. Phys. J.* **C24**, pp. 345–360, doi:10.1007/s10052-002-0953-7, arXiv:hep-ex/0201043 [hep-ex].

Chekanov, S. *et al.* (2003). Measurement of the open charm contribution to the diffractive proton structure function, *Nucl. Phys.* **B672**, pp. 3–35, doi:10.1016/j.nuclphysb.2003.09.001, arXiv:hep-ex/0307068 [hep-ex].

Chekanov, S. *et al.* (2007a). Exclusive rho0 production in deep inelastic scattering at HERA, *PMC Phys.* **A1**, p. 6, doi:10.1186/1754-0410-1-6, arXiv:0708.1478 [hep-ex].

Chekanov, S. *et al.* (2007b). Photoproduction of events with rapidity gaps between jets at HERA, *Eur. Phys. J.* **C50**, pp. 283–297, doi:10.1140/epjc/s10052-007-0241-7, arXiv:hep-ex/0612008 [hep-ex].

Chekanov, S. *et al.* (2009a). A Measurement of the Q**2, W and t dependences of deeply virtual Compton scattering at HERA, *JHEP* **05**, p. 108, doi:10.1088/1126-6708/2009/05/108, arXiv:0812.2517 [hep-ex].

Chekanov, S. *et al.* (2009b). Deep inelastic scattering with leading protons or large rapidity gaps at HERA, *Nucl. Phys.* **B816**, pp. 1–61, doi:10.1016/j.nuclphysb.2009.03.003, arXiv:0812.2003 [hep-ex].

Chekanov, S. *et al.* (2010). Measurement of J/psi photoproduction at large momentum transfer at HERA, *JHEP* **05**, p. 085, doi:10.1007/JHEP05(2010)085, arXiv:0910.1235 [hep-ex].

Ciafaloni, M. (1988). Coherence Effects in Initial Jets at Small q**2 / s, *Nucl. Phys.* **B296**, pp. 49–74, doi:10.1016/0550-3213(88)90380-X.

Ciafaloni, M. and Camici, G. (1998). Energy scale(s) and next-to-leading BFKL equation, *Phys. Lett.* **B430**, pp. 349–354, doi:10.1016/S0370-2693(98)00551-6, arXiv:hep-ph/9803389 [hep-ph].

Collins, J. C. and Ellis, R. K. (1991). Heavy quark production in very high-energy hadron collisions, *Nucl. Phys.* **B360**, pp. 3–30, doi:10.1016/0550-3213(91)90288-9.

Cudell, J. R., Kang, K., and Kim, S. K. (1997). Simple pole fits to p p and anti-p p total cross-sections and real parts, *Phys. Lett.* **B395**, pp. 311–331, doi:10.1016/S0370-2693(97)00046-4, arXiv:hep-ph/9601336 [hep-ph].

De Rujula, A., Glashow, S. L., Politzer, H. D., Treiman, S. B., Wilczek, F., and Zee, A. (1974). Possible NonRegge Behavior of Electroproduction Structure Functions, *Phys. Rev.* **D10**, p. 1649, doi:10.1103/PhysRevD.10.1649.

Derrick, M. *et al.* (1993a). Measurement of the proton structure function F2 in e p scattering at HERA, *Phys. Lett.* **B316**, pp. 412–426, doi:10.1016/0370-2693(93)90347-K.

Derrick, M. *et al.* (1993b). Observation of events with a large rapidity gap in deep inelastic scattering at HERA, *Phys. Lett.* **B315**, pp. 481–493, doi:10.1016/0370-2693(93)91645-4.

Dokshitzer, Y. L. (1977). Calculation of the Structure Functions for Deep Inelastic Scattering and e+ e- Annihilation by Perturbation Theory in Quantum Chromodynamics. *Sov. Phys. JETP* **46**, pp. 641–653, [Zh. Eksp. Teor. Fiz.73,1216(1977)].

Donnachie, A. and Landshoff, P. V. (1992). Total cross-sections, *Phys. Lett.* **B296**, pp. 227–232, doi:10.1016/0370-2693(92)90832-O, arXiv:hep-ph/9209205 [hep-ph].

Dulat, S., Hou, T.-J., Gao, J., Guzzi, M., Huston, J., Nadolsky, P., Pumplin, J., Schmidt, C., Stump, D., and Yuan, C. P. (2016). New parton distribution functions from a global analysis of quantum chromodynamics, *Phys. Rev.* **D93**, 3, p. 033006, doi:10.1103/PhysRevD.93.033006, arXiv:1506.07443 [hep-ph].

Edli, E. *et al.* (2018). Acceleration of electrons in the plasma wakefield of a proton bunch, *Nature* **561**, p. 363.

Enberg, R., Ingelman, G., and Motyka, L. (2002). Hard color singlet exchange and gaps between jets at the Tevatron, *Phys. Lett.* **B524**, pp. 273–282, doi:10.1016/S0370-2693(01)01379-X, arXiv:hep-ph/0111090 [hep-ph].

Fadin, V. S. and Lipatov, L. N. (1998). BFKL pomeron in the next-to-leading approximation, *Phys. Lett.* **B429**, pp. 127–134, doi:10.1016/S0370-2693(98)00473-0, arXiv:hep-ph/9802290 [hep-ph].

Feinberg, E. L. and Pomerančuk, I. (1956). High energy inelastic diffraction phenomena, *Il Nuovo Cimento* **3**, 4, pp. 652–671, doi:10.1007/BF02746068.

Flett, C. A., Jones, S. P., Martin, A. D., Ryskin, M. G., and Teubner, T. (2019). Towards a determination of the low x gluon via exclusive J/ψ production, *PoS* **DIS2019**, p. 053, doi:10.22323/1.352.0053, arXiv:1907.06471 [hep-ph].

Forshaw, J. and Ross, D. (1997). *Quantum Chromodynamics and the Pomeron (Cambridge Lecture Notes in Physics)* (Cambridge University Press), doi:10.1017/CBO9780511524387.

Forshaw, J. R. and Poludniowski, G. (2003). Vector meson photoproduction at high t and comparison to HERA data, *Eur. Phys. J.* **C26**, pp. 411–415, doi:10.1140/epjc/s2002-01078-1, arXiv:hep-ph/0107068 [hep-ph].

Forshaw, J. R. and Ryskin, M. G. (1995). Diffractive vector meson production at large momentum transfer, *Z. Phys.* **C68**, pp. 137–148, doi:10.1007/BF01579812, arXiv:hep-ph/9501376 [hep-ph].

Forte, S., Garrido, L., Latorre, J. I., and Piccione, A. (2002). Neural network parametrization of deep inelastic structure functions, *JHEP* **05**, p. 062, doi:10.1088/1126-6708/2002/05/062, arXiv:hep-ph/0204232 [hep-ph].

Frankfurt, L., McDermott, M., and Strikman, M. (2001). A Fresh look at diffractive J / psi photoproduction at HERA, with predictions for THERA, *JHEP* **03**, p. 045, doi:10.1088/1126-6708/2001/03/045, arXiv:hep-ph/0009086 [hep-ph].

Golec-Biernat, K. J. and Wusthoff, M. (1998). Saturation effects in deep inelastic scattering at low Q**2 and its implications on diffraction, *Phys. Rev.* **D59**, p. 014017, doi:10.1103/PhysRevD.59.014017, arXiv:hep-ph/9807513 [hep-ph].

Goulianos, K. A. (1983). Diffractive Interactions of Hadrons at High-Energies, *Phys. Rept.* **101**, p. 169, doi:10.1016/0370-1573(83)90010-8.

Gribov, L. V., Levin, E. M., and Ryskin, M. G. (1983). Semihard Processes in QCD, *Phys. Rept.* **100**, pp. 1–150, doi:10.1016/0370-1573(83)90022-4.

Gribov, V. N. and Lipatov, L. N. (1972a). Deep inelastic e p scattering in perturbation theory, *Sov. J. Nucl. Phys.* **15**, pp. 438–450, [Yad. Fiz.15,781(1972)].

Gribov, V. N. and Lipatov, L. N. (1972b). e+ e- pair annihilation and deep inelastic e p scattering in perturbation theory, *Sov. J. Nucl. Phys.* **15**, pp. 675–684, [Yad. Fiz.15,1218(1972)].

Harland-Lang, L. A., Martin, A. D., Motylinski, P., and Thorne, R. S. (2015). Parton distributions in the LHC era: MMHT 2014 PDFs, *Eur. Phys. J.* **C75**, 5, p. 204, doi:10.1140/epjc/s10052-015-3397-6, arXiv:1412.3989 [hep-ph].

Ingelman, G. and Schlein, P. E. (1985). Jet Structure in High Mass Diffractive Scattering, *Phys. Lett.* **152B**, pp. 256–260, doi:10.1016/0370-2693(85)91181-5.

Jung, H. (1995). Hard diffractive scattering in high-energy e p collisions and the Monte Carlo generator RAPGAP, *Comput. Phys. Commun.* **86**, pp. 147–161, doi:10.1016/0010-4655(94)00150-Z.

Jung, H. (2002). The CCFM Monte Carlo generator CASCADE, *Comput. Phys. Commun.* **143**, pp. 100–111, doi:10.1016/S0010-4655(01)00438-6, arXiv:hep-ph/0109102 [hep-ph].

Jung, H. and Salam, G. P. (2001). Hadronic final state predictions from CCFM: The

Hadron level Monte Carlo generator CASCADE, *Eur. Phys. J.* **C19**, pp. 351–360, doi:10.1007/s100520100604, arXiv:hep-ph/0012143 [hep-ph].

Jung, H. (2020). Aspects of BFKL Physics at HERA, To appear elsewhere in this volume.

Kaidalov, A. B. (1979). Diffractive Production Mechanisms, *Phys. Rept.* **50**, pp. 157–226, doi:10.1016/0370-1573(79)90043-7.

Khanpour, H. (2019). Phenomenology of diffractive DIS in the framework of fracture functions and determination of diffractive parton distribution functions, *Phys. Rev.* **D99**, 5, p. 054007, doi:10.1103/PhysRevD.99.054007, arXiv:1902.10734 [hep-ph].

Khoze, D. and Ryskin, M and Tasevsky, M. (2020). High Energy Soft QCD and Diffraction, Chapter to appear in the 2020 PDG review, in litt.

Klein, M. and Yoshida, R. (2008). Collider Physics at HERA, *Prog. Part. Nucl. Phys.* **61**, pp. 343–393, doi:10.1016/j.ppnp.2008.05.002, arXiv:0805.3334 [hep-ex].

Kowalski, H., Motyka, L., and Watt, G. (2006). Exclusive diffractive processes at HERA within the dipole picture, *Phys. Rev.* **D74**, p. 074016, doi:10.1103/PhysRevD.74.074016, arXiv:hep-ph/0606272 [hep-ph].

Kuraev, E. A., Lipatov, L. N., and Fadin, V. S. (1976). Multi - Reggeon Processes in the Yang-Mills Theory, *Sov. Phys. JETP* **44**, pp. 443–450, [Zh. Eksp. Teor. Fiz.71,840(1976)].

Kuraev, E. A., Lipatov, L. N., and Fadin, V. S. (1977). The Pomeranchuk Singularity in Nonabelian Gauge Theories, *Sov. Phys. JETP* **45**, pp. 199–204, [Zh. Eksp. Teor. Fiz.72,377(1977)].

Levin, E. M., Ryskin, M. G., Shabelski, Yu. M., and Shuvaev, A. G. (1991). Heavy quark production in semihard nucleon interactions, *Sov. J. Nucl. Phys.* **53**, p. 657, [Yad. Fiz.53,1059(1991)].

Levy, A. (2009). Electroproduction of Vector Mesons, in *Proceedings, 17th International Workshop on Deep-Inelastic Scattering and Related Subjects (DIS 2009): Madrid, Spain, April 26-30, 2009*, p. 177, arXiv:0907.2178 [hep-ex].

LHeC Study Group (2020). The Large Hadron-electron Collider at the LHeC, Extensive update to the LHeC CDR, CERN-Acc-Note-2020-0002, in litt.

Lipatov, L. N. (1975). The parton model and perturbation theory, *Sov. J. Nucl. Phys.* **20**, pp. 94–102, [Yad. Fiz.20,181(1974)].

Lipatov, L. N. (1986). The Bare Pomeron in Quantum Chromodynamics, *Sov. Phys. JETP* **63**, pp. 904–912, [Zh. Eksp. Teor. Fiz.90,1536(1986)].

Lipatov, L. N. (1997). Small x physics in perturbative QCD, *Phys. Rept.* **286**, pp. 131–198, doi:10.1016/S0370-1573(96)00045-2, arXiv:hep-ph/9610276 [hep-ph].

Lonnblad, L. (1992). ARIADNE version 4: A Program for simulation of QCD cascades implementing the color dipole model, *Comput. Phys. Commun.* **71**, pp. 15–31, doi:10.1016/0010-4655(92)90068-A.

Low, F. E. (1975). A Model of the Bare Pomeron, *Phys. Rev.* **D12**, pp. 163–173, doi:10.1103/PhysRevD.12.163.

Marchesini, G. (1995). QCD coherence in the structure function and associated distributions at small x, *Nucl. Phys.* **B445**, pp. 49–80, doi:10.1016/0550-3213(95)00149-M, arXiv:hep-ph/9412327 [hep-ph].

Martin, A. D., Nockles, C., Ryskin, M. G., and Teubner, T. (2008). Small x gluon from exclusive J/psi production, *Phys. Lett.* **B662**, pp. 252–258, doi:10.1016/j.physletb.2008.02.067, arXiv:0709.4406 [hep-ph].

Martin, A. D., Ryskin, M. G., and Teubner, T. (1997). The QCD description of diffractive rho meson electroproduction, *Phys. Rev.* **D55**, pp. 4329–4337, doi:10.1103/PhysRevD.55.4329, arXiv:hep-ph/9609448 [hep-ph].

Martin, A. D., Ryskin, M. G., and Teubner, T. (2000). Q**2 dependence of diffractive

vector meson electroproduction, *Phys. Rev.* **D62**, p. 014022, doi:10.1103/PhysRevD.62.014022, arXiv:hep-ph/9912551 [hep-ph].

Mueller, A. H. (1990). Small x Behavior and Parton Saturation: A QCD Model, *Nucl. Phys.* **B335**, pp. 115–137, doi:10.1016/0550-3213(90)90173-B.

Mueller, A. H. and Tang, W.-K. (1992). High-energy parton-parton elastic scattering in QCD, *Phys. Lett.* **B284**, pp. 123–126, doi:10.1016/0370-2693(92)91936-4.

Newman, P. (2004). Deep inelastic lepton nucleon scattering at HERA, *Int. J. Mod. Phys.* **A19**, pp. 1061–1073, doi:10.1142/S0217751X0401897X, arXiv:hep-ex/0312018 [hep-ex].

Newman, P. and Wing, M. (2014). The Hadronic Final State at HERA, *Rev. Mod. Phys.* **86**, 3, p. 1037, doi:10.1103/RevModPhys.86.1037, arXiv:1308.3368 [hep-ex].

Nussinov, S. (1975). Colored Quark Version of Some Hadronic Puzzles, *Phys. Rev. Lett.* **34**, pp. 1286–1289, doi:10.1103/PhysRevLett.34.1286.

Salam, G. P. and Soyez, G. (2007). A Practical Seedless Infrared-Safe Cone jet algorithm, *JHEP* **05**, p. 086, doi:10.1088/1126-6708/2007/05/086, arXiv:0704.0292 [hep-ph].

Sirunyan, A. M. *et al.* (2019a). Measurement of exclusive $\rho(770)^0$ photoproduction in ultraperipheral pPb collisions at $\sqrt{s_{\mathrm{NN}}} = 5.02$ TeV, *Eur. Phys. J.* **C79**, 8, p. 702, doi:10.1140/epjc/s10052-019-7202-9, arXiv:1902.01339 [hep-ex].

Sirunyan, A. M. *et al.* (2019b). Measurement of exclusive Υ photoproduction from protons in pPb collisions at $\sqrt{s_{\mathrm{NN}}} = 5.02$ TeV, *Eur. Phys. J.* **C79**, 3, p. 277, doi:10.1140/epjc/s10052-019-6774-8, arXiv:1809.11080 [hep-ex].

Stasto, A. M. (2020). Contribution to Lev Lipatov's Memorial Book, To appear elsewhere in this volume.

Ullrich, T. (2019). Luminosity v Energy plot (after M. Klein). Private Communication.